

# Introducing a precast moment resistant beam-to-column concrete connection comparable with in-situ one

Jamshid Esmaeili\* and Neyram Ahooghalandary<sup>a</sup>

Department of Civil Engineering, University of Tabriz, Tabriz, 29 Bahman Avenue, Iran

(Received July 15, 2018, Revised January 13, 2019, Accepted March 11, 2019)

**Abstract.** Precast reinforced concrete structure (PRCS) consists of prefabricated members assembled at worksites and has more connections limitations in comparison with the equivalent in-situ reinforced concrete structure (IRCS). As a result of these limitations, PRCSs have less ductility in comparison with IRCSs. Recent studies indicate that the most noticeable failure in PRCSs have occurred in their connection zone. The objective of this study is introducing a type of precast beam-to-column connection (PBC) which in spite of being simple is of the same efficiency and performance as in-situ beam-to-column connection (IBC). To achieve this, the performance of proposed new PBC at exterior joint of a four story PRCS was analyzed by pseudo dynamic analysis and compared with that of IBC in equivalent IRCS. Results indicated that the proposed connection has even better performance in terms of strength, energy dissipation and stiffness, than that of IBC.

**Keywords:** finite element analysis, precast connection, beam-to-column connection, precast structure

## 1. Introduction

Reinforced concrete precast members have high quality in comparison with in-situ ones and lead to save in time and costs in construction process. However, the PRCS has not reached its full potential yet. The problems are mainly due to the connection deficiency between the prefabricated members.

While many experimental and numerical studies have been performed on the behavior of IBC under cyclic loading, few studies have been conducted on the performance of PBC among which, the contribution of moment resistant PBC is negligible. The main issue is related to energy dissipation and moment resistance in PBCs. PRCSs have less ductile performance in their connections and plastic hinges under applied loads.

Studies on PBC have been conducted using experimental and numerical models. In the case of “dry” PBC (in which anchorage plates are welded or bolted without the use of cast-in-place concrete), Rodriguez and Torres (2013) studied common PBCs in Mexico. These connections were used for precast moment frames. Here, the welded bars between the ended anchorage plates in the beam and column elements provided necessary connection. The results showed that using longitudinal welded bars decrease the ductility in joint area and result in premature failure. Similar investigations have been carried out by Hong *et al.* (2010), Ghayeb *et al.* (2017), Fan and Lu (2008). With regard to semi monolithic PBC (in which cast-

in-place concrete is used), Choi *et al.* (2013) tested one IBC and four PBCs under seismic loading. Joint details were investigated to achieve structural integrity and special reinforcement layout in the connection zone. Generally, the performance of beam-to-column connections was desirable and the average strength of the PBCs was about 1.15 times the strength of the IBC. Additionally, the behavior of joints was evaluated to be ductile. Im *et al.* (2013), Kataoka *et al.* (2015) also studied similar connections and reported their acceptable performance. However, other researchers such as Maya *et al.* (2013) have considered these connections to be inefficient, and thus tried to use a fiber-reinforced concrete in order to achieve a better performance. After all, in spite of the obtained results in previous researches, the semi monolithic PBC need to be casted in place which, in and of itself, is in contradiction with the purpose of prefabricating and make this process last long. Another type of PBCs is hybrid ones. In the case of hybrid precast PBC (in which post-tensioned cables are used). Hawileh *et al.* (2010) chose a 3D finite element model to study. The model was proposed to consider the effects of pre-stressing in post-tensioned cables and nonlinear concrete behavior. The results showed that the yielding of longitudinal bars caused failure in the joint area and the finite element was considered to be a proper method for assessment of the PBCs behavior. In this field, similar studies have been done by Bradley *et al.* (2008), Guan *et al.* (2016), Cheng (2007). However, in these studies, like previous ones, references to the assembling requirement of the proposed connection are not available and the process of installation and production is ambiguous. Moreover, in most of the studies, beam-to-floor connection requirements have not been considered in precast concrete beams, especially in high seismic zones. Due to the mentioned problems of PBCs, this study tried to provide an efficient and simple connection in the production

\*Corresponding author, Associate Professor  
E-mail: [j-esmaeili@tabrizu.ac.ir](mailto:j-esmaeili@tabrizu.ac.ir)

<sup>a</sup>Ph.D. Student  
E-mail: [ahooghalandary@tabrizu.ac.ir](mailto:ahooghalandary@tabrizu.ac.ir)

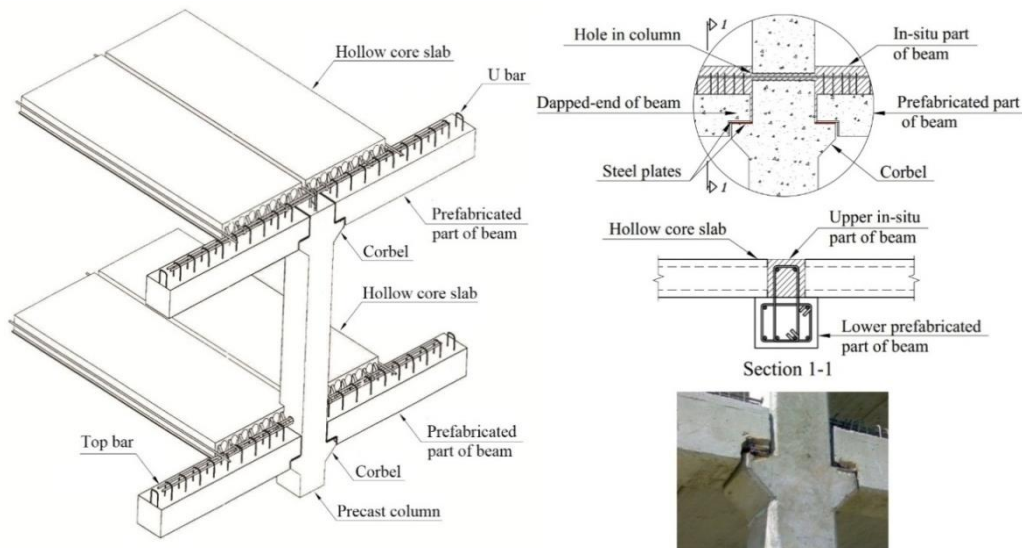
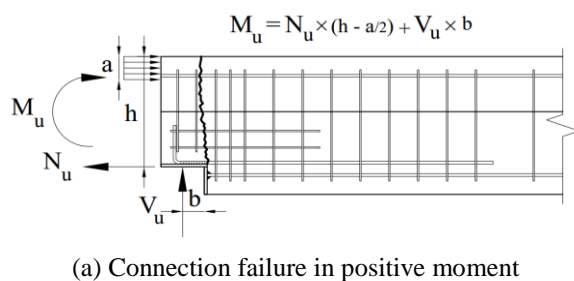


Fig. 1 Conventional PBC



(a) Connection failure in positive moment



(b) An example of connection failure

Fig. 2 Typical failure mechanism of PBC

and considered the requirements of assembling and structural integrity.

## 2. Conventional PBC

PBCs are usually used with corbel. Corbel plays a bearing role in the joint area for the beam, and also provides a solution to remove the tight tolerances. An example of this type of joint is shown in Fig. 1.

This connection is a combination of dry and semi monolithic PBCs. The lower part of the beam-to-column joint is considered dry due to the ease of construction. In this part, the connection is made by welding steel plate on corbel to bottom steel plate at the end of the precast beam. Using corbel in this part also helps easier installation. The beam is built with dapped-end connection at its end in order to not to decrease ceiling height. After completion of the bottom part of the joint, hollow core slabs are placed on the lower prefabricated part of the precast beam. In the upper part, the connection is completed through passing of the bars from the holes in column and finally, concrete is casted in place. This part of beam has less width so that the hollow core slabs could be placed on the prefabricated part. In spite of requiring cast-in-place concrete in the upper part of the beam, the mold is not needed due to the confinement of the lower face by the prefabricated part and the sides by the hollow core slabs.

The reduced cross section in the dapped end of beam results in less lever arm and the connection could not carry the beam flexural capacity especially under positive moment (Fig. 2(a)). So, this type of connection is not used alone in moment resistant frames and another lateral resistant system is required. Fig. 2(b) shows an example of failure in these connections.

## 3. Introduction of proposed connection

In order to study the proposed PBC and compare it with the in-situ one, a four story residential building with a lateral bearing system in the form of intermediate moment frame was designed by spectral dynamic analysis. This structure was designed according to the seismic criteria of Standard No. 2800 (2014), in a region with a very high seismic zone. This structure was proposed and designed with a story height of 3.2 meters and 4 bays with the length of 6 meters. The model was assumed to be symmetrical. The applied loads to the structure included dead, live and earthquake loads. Modeled beams and columns were detailed in a way to provide seismic requirements for intermediate moment frame elements. To evaluate the connection joint performance, an exterior joint was selected from the internal frame of this structure on its third floor. According to the applied load on the selected joint, it was designed in two in-situ and precast cases with a scale of 2/3

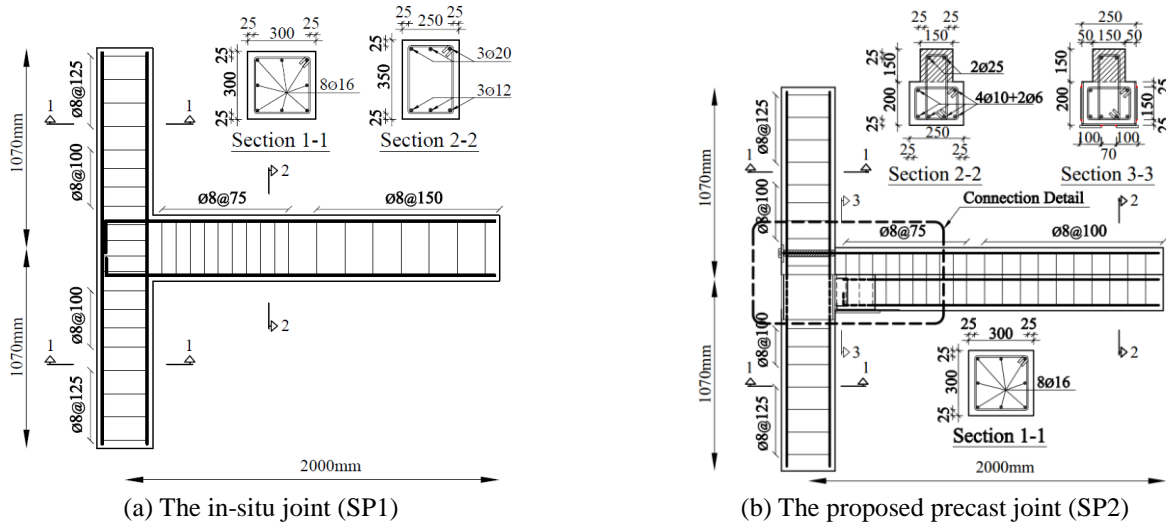


Fig. 3 Configuration of the designed joints

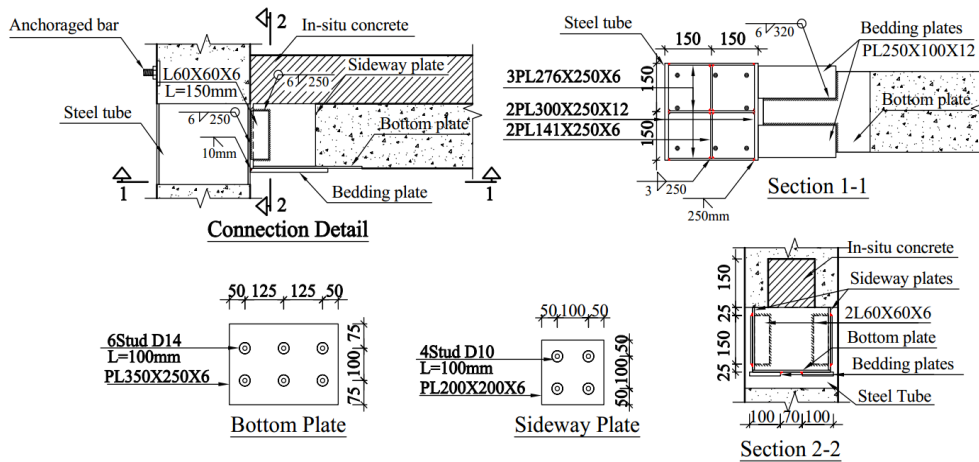


Fig. 4 Details and dimensions of the SP2 parts

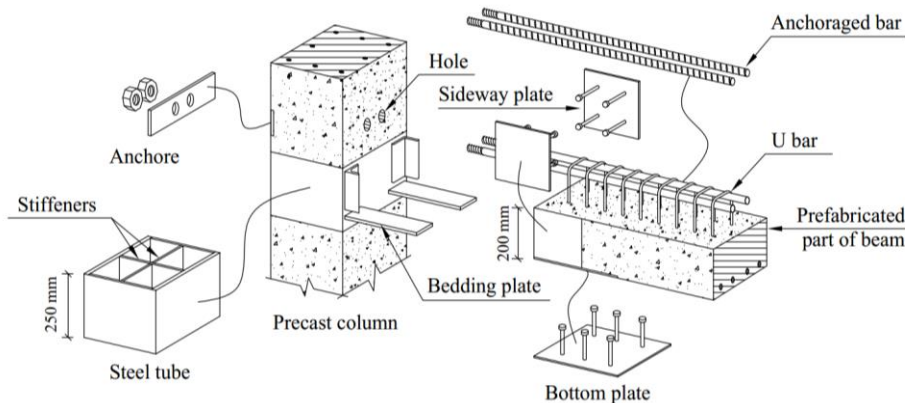


Fig. 5 Different parts of SP2 Connection

using the ACI318-14 (2014) and PCI design handbook (2010). In designing the joint, flexural and shear capacity, anchorage length, capacity of axial force and moment interaction in column, shear capacity of column and requirements for stirrups of intermediate moment frames were considered. Figs. 3(a)-(b) show the configuration of the in-situ (SP1) and proposed precast joints (SP2)

respectively. More details of the SP2 parts are shown in Figs. 4-5. In the SP2, instead of using corbel in the lower part, the two bedding plates connected to the peripheral steel tube of the column were used. These plates, in addition to eliminating the dapped part of the beam, provided a better condition for connection between the lower end parts of beam to column for resisting positive moment. The steel

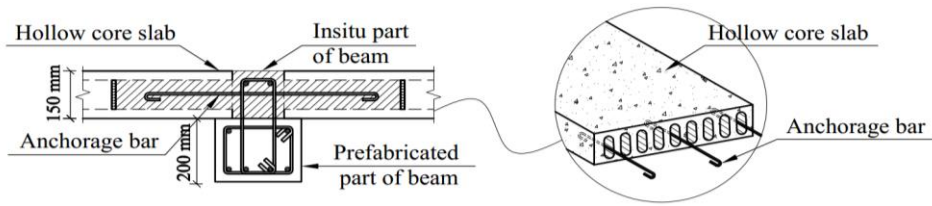


Fig. 6 Connection detail of the precast beam to hollow core slabs with anchorage bars

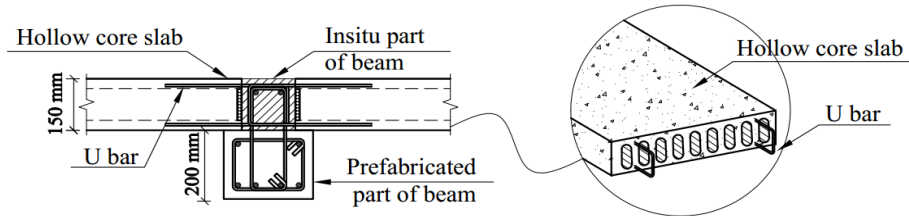


Fig. 7 Connection detail of the precast beam to hollow core slabs with U bars

tube has been also connected to the cruciform stiffeners buried in the column concrete. Welding the bottom plate to the bedding plates at the end of the beam complemented the connection in this part. In the upper part, the holes in the beam-to-column joint were used to pass the longitudinal bars which are mechanically anchored on the opposite face and after casting, filled with concrete. In addition, shearing effort in the joint area was resisted through welding steel angle to anchorage sideways plates of the beam in one side and column steel tube on the other side. The bottom and sideways plates were anchored by studs to the concrete of the beam.

The proposed inverse *T* shape precast beam provides a condition for hollow core slabs to be placed easily on the bottom part of it. After placement of the slab and anchorage bar at specific distances in the holes, the upper part of beam is casted without any requirement for mold according to Fig. 6. The other method is to use hollow core slabs with *U* shape bars at their ends. In this method after the placement of hollow core slab, upper longitudinal bars of the beam pass through *U* bars and then concrete is casted according to Fig. 7.

The advantages of using such PBC in the production and installation process are as follows:

- Eliminating corbel of column and avoid wasting ceiling height.
- Creating suitable bedding for bearing of precast beam by installing the bedding plates at the connection zone and also creating suitable conditions for positive moment resisting.
- Easy producing of precast columns in the factory due to eliminating the corbel.
- Easier fabrication of precast beam because of eliminating the dapped part of beam.
- No need to use molds for casting the upper part of beam after the placement of hollow core slabs.

#### 4. Material modeling

Studying the performance of the connections through

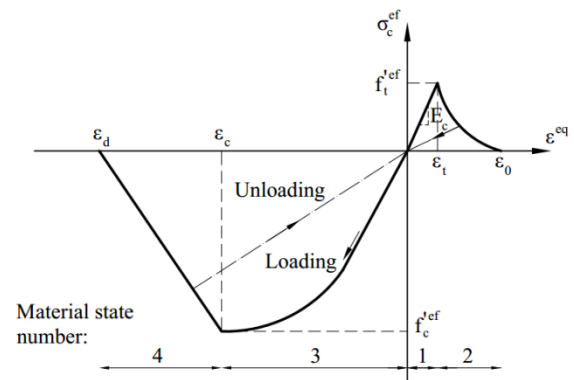


Fig. 8 The suggested concrete model of CEB-FIP

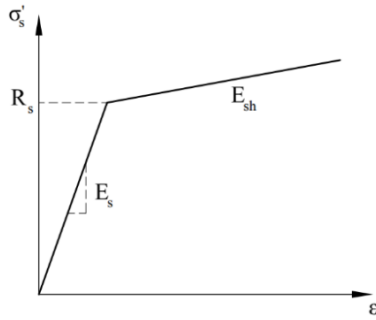
nonlinear finite element analysis requires the precise definition of idealized material specification. To this end, in each special case, suggested models of other researchers were used.

In order to determine the stress-strain curve of concrete, proposed CEB-FIP (1990) modeling was used. The presented curve by this code consisted of four parts and is shown in Fig. 8.

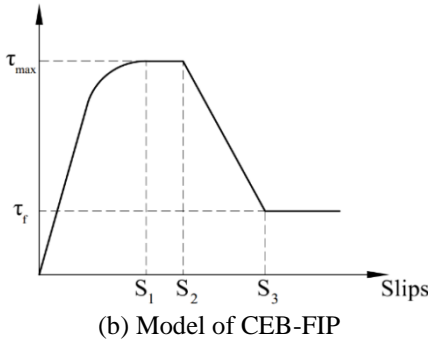
- Tension region before cracking: The behavior of concrete in this region was considered as a material with linear elastic properties.  $E_c$ , elastic modulus of concrete and  $f_t^{ef}$ , effective tensile strength, were derived from the biaxial failure function.
- Tensile region after cracking: For this area, the exponential crack opening function of Hordijk (1991) obtained experimentally, was used.
- Compression region before peak stress: The equation proposed for this region is in accordance with the model provided by CEB-FIP for concrete. This equation is capable of considering a wide range of diagrams from linear to curve. In this section,  $f_c^{ef}$  is the effective compression strength of concrete, and  $\epsilon_c$  is the strain in peak stress.
- Compression region after peak stress: In this study, a fictitious compression plane model was used for this

Table 1 Concrete parameters

Parameter	Definition	Relation	Value	Unit
$f'_c$	Compressive strength	$f'_c = -0.85 f'_{cu}$	30	MPa
$f'_t$	Tensile strength	$f'_t = 0.24 (f'_{cu})^{2/3}$	2.58	MPa
$E_c$	Elastic modulus	$E_c = (6000 - 15.5 f'_{cu}) \times (f'_{cu})^{1/2}$	3.24E+4	MPa
$\nu$	Poisson's ratio	-	0.20	-
$w_d$	Critical compressive displacement	-	0.50	mm
$G_f$	Specific fracture energy	-	6.45E-5	MPa/mm



(a) Bilinear curve with strain hardening



(b) Model of CEB-FIP

Fig. 9 The selected curves for reinforcing bar in concrete

region. This theory is confirmed by Van Mair's (1986) experiments.  $\varepsilon_d$  in this region represents the strain equivalent to zero stress.

Table 1 lists the defined parameters for concrete modeling. Biaxial stress failure criterion of concrete was considered in accordance with the relations presented by Kupfer and Gerstle (1973).

For modeling the reinforcing bars, a "discrete model" was used. In this model, the rebar is considered independent of concrete and in contact with it. The ideal tension curve of the reinforcing bars and steel parts were defined bilinear by regarding strain hardening ( $E_{sh}$ ) equal to 2% of the initial elastic modulus ( $E_s$ ) as shown in Fig. 9(a). The necessary parameters values for longitudinal and transverse bars are indicated in Table 2.

To consider the reinforcement bonding to concrete, the model provided by CEB-FIP code was used. The diagram

Table 2 Reinforcing bars and steel parts parameters

Parameter	Definition	Longitudinal reinforcements	Transvers reinforcements	Steel parts	Unit
$E_s$	Elastic modulus	2.10E+5	2.10E+5	2.10E+5	MPa
$E_{sh}$	Strain hardening	4200	4200	4200	MPa
$\sigma_y$	Yield strength	400	300	240	MPa
$\sigma_u$	Yield strain	0.002	0.002	0.002	-
$\varepsilon_f$	Failure strain	0.14	0.19	0.20	-
$\nu$	Poisson's ratio	-	-	0.3	-

Table 3 Bond-slip parameters

Parameter	Definition	Relation or explanation	Value	Unit
$S_1$	According to Fig.9(b)	Good bond condition	1	mm
$S_2$	According to Fig.9(b)	Good bond condition	3	mm
$S_3$	Clear rib spacing	Good bond	According to	mm
$\alpha$	-	Ribbed bar	0.40	-
$\tau_{max}$	Maximum shear strength	$2.5\sqrt{f'_c}$	13.69	MPa
$\tau_f$	Failure shear	$0.4 \tau_{max}$	5.48	MPa

presented in the CEB-FIP is shown in Fig. 9(b). The diagram has divided to four parts as below

$$\tau = \tau_{max} \left( \frac{S}{S_1} \right)^\alpha, 0 \leq S \leq S_1 \quad (1)$$

$$\tau = \tau_{max}, S_1 \leq S \leq S_2 \quad (2)$$

$$\tau = \tau_{max} - (\tau_{max} - \tau_f) \times \left( \frac{S - S_1}{S_3 - S_2} \right), S_2 \leq S \leq S_3 \quad (3)$$

$$\tau = \tau_f, S_3 \leq S \quad (4)$$

In this relations  $S_1$ ,  $S_2$  and  $S_3$  are parameters defined based on compressive strength of concrete, reinforcement diameter and reinforcement type. The other important parameters are the confinement condition and quality of concrete casting. In this research, the parameters were selected based on the type of ribbed bar with good bond confinement condition. Table 3 shows the constituent parameters of bond-slip reinforcement.

To define steel segments, plasticity model of Von Mises (1982) was used, which is also called the plasticity model  $J_2$  and is based on the parameter  $k$ . The yield function in this model is defined as follows

$$F^P(\sigma_{ij}) = \sqrt{J_2} - k(\varepsilon_{eq}^P) = 0 \quad (5)$$

In this relation,  $J_2$  refers to the second invariant of stress deviator tensor. The parameter  $k$  is the maximum shear stress as follows

$$k(\varepsilon_{eq}^P) = \sigma_y + H\varepsilon_{eq}^P \quad (6)$$

Table 4 Interfaces parameters for SP2

Parameter	Definition	Relation or explanation	Value	Unit
Interface between in situ and precast concrete				
$C$	Cohesion	Concrete shear strength	9.18	MPa
$\phi$	Angle of internal friction	Concrete to harden concrete condition	0.6	-
Interface between sideway plate and concrete				
$C$	Cohesion	Equivalent resistance base on anchors (studs) shear strength	25.35	MPa
$\phi$	Angle of internal friction	Concrete to harden concrete with roughened surface condition	0.7	-
Interface between bottom plate and concrete				
$C$	Cohesion	Equivalent resistance based on anchors (studs) shear strength	34.32	MPa
$\phi$	Angle of internal friction	Concrete to harden concrete with roughened surface condition	0.7	-
Interface between bedding plate and bottom plate				
$C$	Cohesion	Equivalent resistance based on welding strength	92.61	MPa
$\phi$	Angle of internal friction	-	0	-
Interface between angle and sideway plate				
$C$	Cohesion	Equivalent resistance based on welding strength	23.15	MPa
$\phi$	Angle of internal friction	-	0	-
Interface between angle and steel tube				
$C$	Cohesion	Equivalent resistance based on welding strength	19.29	MPa
$\phi$	Angle of internal friction	-	0	-

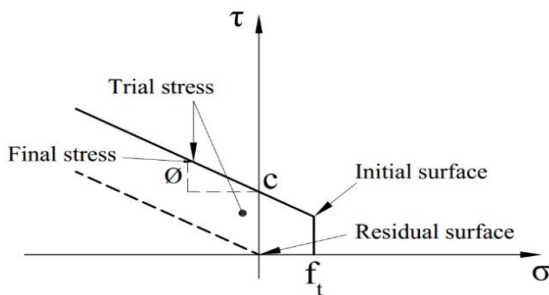


Fig. 10 The curve based on the Mohr-Coulomb theory for interface

The parameter  $H$  is the gradient of hardening modulus of steel.

At the interfaces, a behavioral model based on the Mohr-Coulomb (1982) criterion was used to simulate the contacts. In this theory, the simulation of the interaction between the two surfaces depends on the interface material as well as the normal and tangent stresses created in the interface. The stress diagram on the interface between elements is shown in Fig. 10 by using the Mohr-Coulomb theory.

The criterion for the initial failure surface in the Mohr-Coulomb theory is obtained from the following equations.

$$|\tau| \leq c - \sigma \cdot \phi, \sigma \leq f_t \quad (7)$$

$$\tau = 0, \sigma > f_t \quad (8)$$

Where  $c$  is the cohesion and  $\phi$  is the angle of internal friction.

After the stresses exceed the resistance at the surface, the interface fails and residual strength will only be due to the friction in residual interface. This model was used to define the interface between the new concrete in the upper part of the beam and the hardened precast concrete in the lower part of it and also, to simulate welding of the bottom

plate to the bedding plates and angles to sideway plates of the beam and column steel tube. Equivalent shear capacity of the studs is modeled in the same way. Table 4 specifies the parameters values associated to the interface of different parts of connection.

## 5. Finite element modeling

Nonlinear finite element analysis was conducted by Atena 3D software. This software is capable of observing nonlinear behavior of materials as well as, determining the stresses and strains in longitudinal reinforcements, stirrups and cracking in concrete.

To use the finite element method in joints analyzing, it is required to define 3D truss elements for one-dimensional members. These are isoperimetric elements integrated by 2 integration points (for the case of quadratic interpolation) for elements with 3 element nodes. These elements are suitable for reinforcing bars in three-dimensional analysis. Further, for 3D members, tetrahedral elements with 10 nodes and brick elements with 20 nodes were used simultaneously. Geometry of the elements is shown in Figs. 11(a)-(c). Tetrahedral element is used in supporting and load bearing members and brick element is used to define 3D members of joints. The modeled joints in the software are shown in Figs. 12(a)-(b) for the both SP1 and SP2.

## 6. Analysis procedure and loading program

Considered layout for loading procedure of the beam-to-column joint in two stages is indicated in Fig. 13(a). The details and dimensions of the joints were shown in Figs. 3(a)-(b). In the first stage, the column was loaded under 700 kN of axial compression load. This load was approximately equal to  $0.1f_c'A_g$  along column axes, where  $f_c'$  and  $A_g$  are the

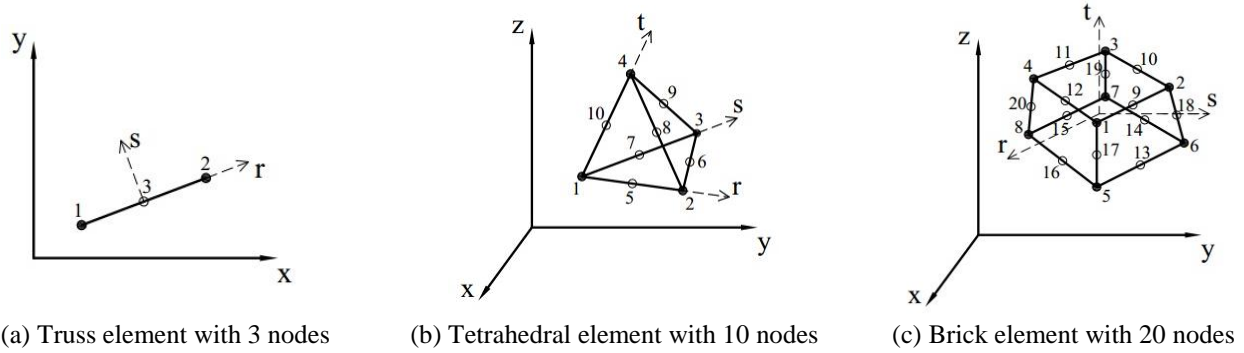


Fig. 11 Finite element components used in the software

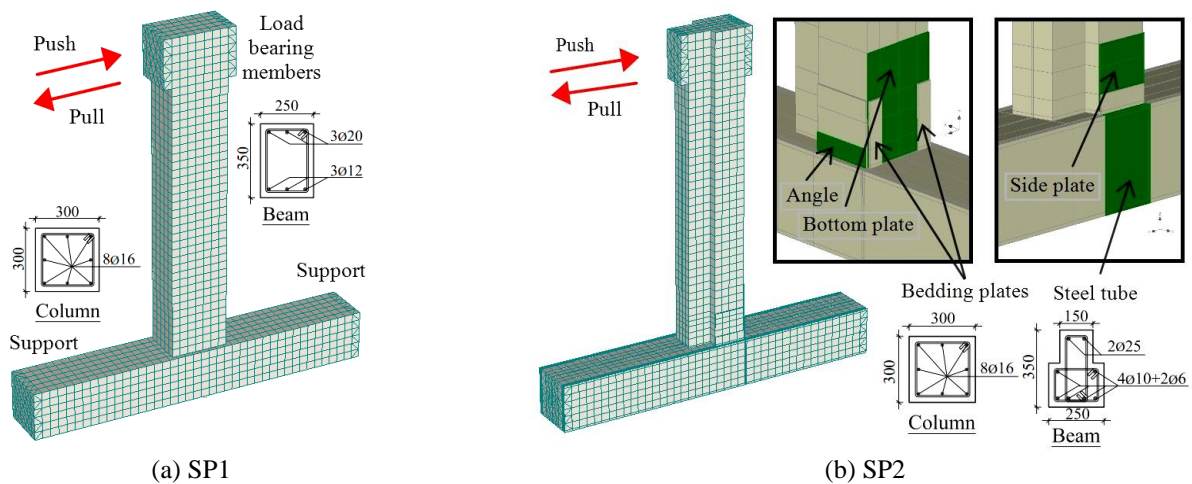
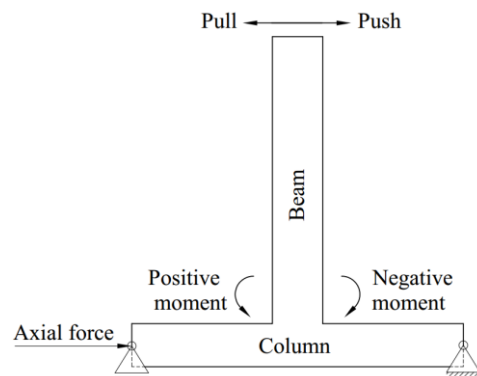


Fig. 12 Finite element modeling in the software

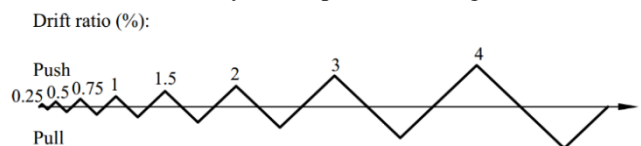
concrete compressive strength and the net cross section of column, respectively. This loading procedure was carried out as a load control process and in 20 steps.

The second stage initiated after the axial load of the column reached 700 kN. In this stage, another cyclic loading was applied to the end of the beam and on two ends of the column. Hinged supports were placed according to the layout shown in Fig. 13(a). These supports were selected to simulate the inflection points of the column, where moment is zero under the applied lateral load. This loading stage was carried out in displacement control process, and at each step, a displacement with a variation of about 1 mm was applied to the end of the beam in two reversed cycles. As shown in Fig. 13(b), the loading was continued in the positive and negative moments until the 4% drift ratio. The selected load pattern is similar to the recommended method of ACI374.1-05 (2005). In this method, the initial drift ratio should be in elastic range. The subsequent drift ratios should be between 1.25 to 1.5 times the previous drift ratios and the test should be continued at least until the drift ratio of 3.5%.

In the loading points and supports, in order to avoid strain concentration and bearing stress, steel plates were used. At loading points, the displacement and applied force at each step were measured. Strains were also determined at certain intervals from the column face on the top and the bottom bars of the beam to determine the plastic hinge position and reinforcement yielding.



(a) Analysis setup and load stages

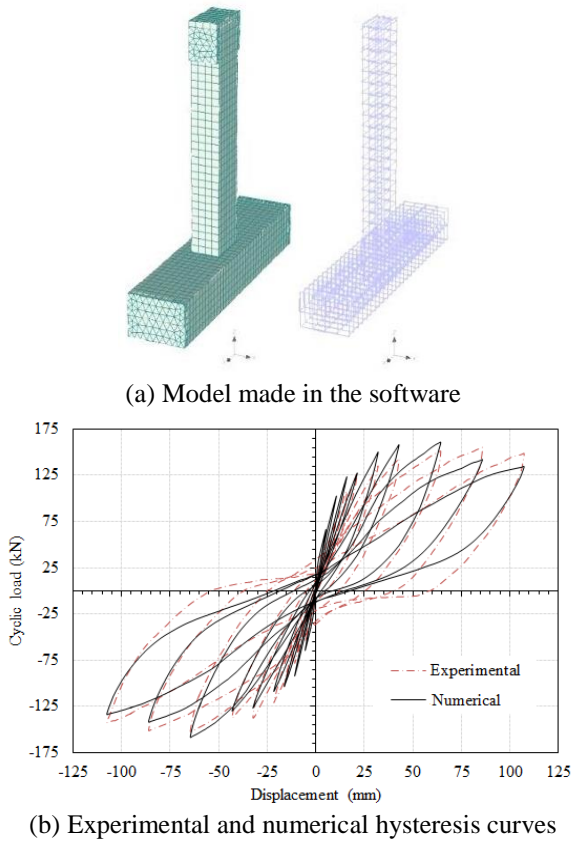


(b) Loading program at the end of the beam

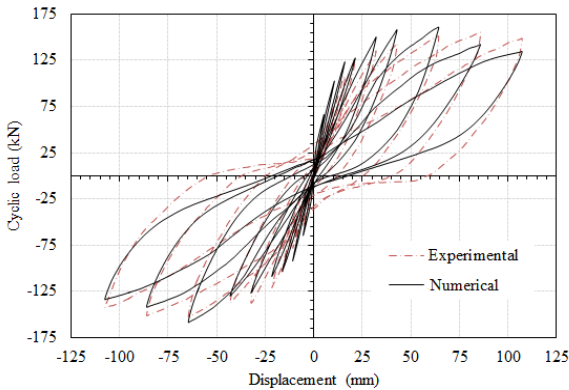
Fig. 13 Considered layout and loading procedure in the software

## 7. Verification of finite element analysis

To validate the modeling and analysis procedure, the experimental model of Lee and Yu's (2009) on exterior IBC was verified by finite element analysis. The selected joint



(a) Model made in the software



(b) Experimental and numerical hysteresis curves

Fig. 14 Verification of analysis

was a specimen named W0. The loading protocol and setup was considered to be in accordance with the test. Figs. 14(a)-(b) shows the model made in the software and the results of the test on the mentioned connection and the analysis performed up to the maximum of 5% drift. The results of the analysis are compared with the third iteration of each cycle.

In Fig. 15, the skeleton curve for two experimental and numerical models is illustrated. The average difference between the maximum resistances in each cycle was 11%. The maximum resistance in the positive moment under testing and the finite element analysis was obtained respectively in 4% and 3% drift. Nevertheless, under the negative moment in the both methods, the maximum resistance was obtained in 3% drift which matches.

The second stiffness in each cycle of the experimental and numerical results was compared. The second stiffness of each cycle was obtained in accordance to the definition of ACI374.1-05 from the slope of passing line from  $-1/10$  to  $1/10$  maximum drift per cycle. The stiffness of 0.25% drift in the diagram is the initial stiffness. The average difference in the results in all cycles was about 17%. Also the initial stiffness from the finite element analysis was 25% more on average than the obtained stiffness from the experimental results. The reason can be attributed to partial wobbling in the test setup at the initial step of the experiment.

Finally energy dissipations were compared in each cycle of loading. The amount of energy dissipated per cycle was derived from its area. The energy dissipation rate in all

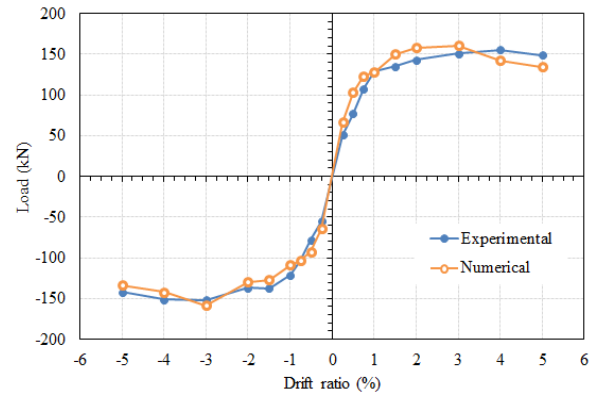
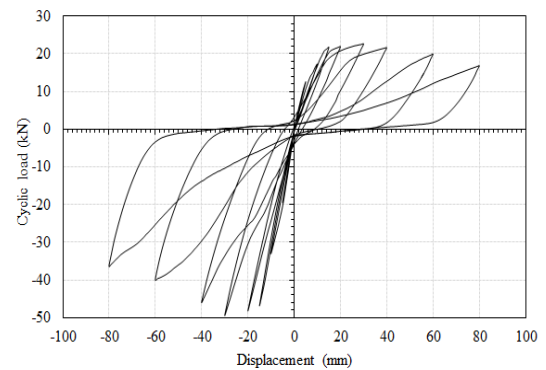
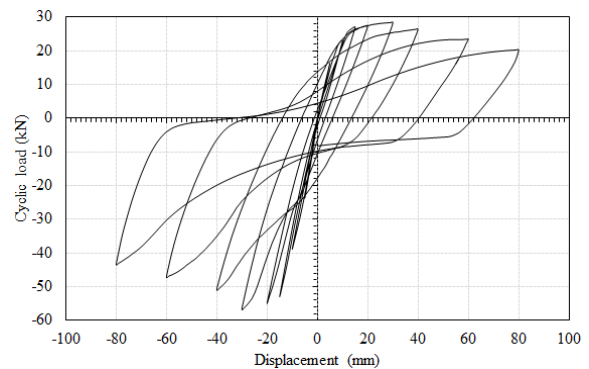


Fig. 15 The skeleton curve for the two experimental and numerical models



(a) SP1



(b) SP2

Fig. 16 Hysteresis curve of the studied connections

cycles under the finite element analysis, compared to the experimental results, showed an average difference of about 24%. The finite element model represented less energy dissipation, especially in the last steps. So it can be stated that the results of the finite element model in term of energy dissipation were more conservative than experimental results.

## 8. Evaluation of pseudo dynamic analysis results

### 8.1 Studying the parameters of the hysteresis diagram

In order to compare the performance of SP1 and SP2, the results of their pseudo dynamic analysis are shown in

Table 5 Summary of the analysis results

Connection	Load carrying capacity*					Deformation capacity				Stiffness	
	Load direction	Maximum resistance ( $P_{max}$ )	Nominal resistance ( $P_n$ )	$P_{max}/P_n$	Maximum joint shear ( $V_{jmax}$ )	Yielding displacement ( $\delta_y$ ) (mm)	Maximum displacement ( $\delta_u$ ) (mm)	Ductility	$k_y$ (kN/mm)	$k_p/k_y$ (%)	
SP1	+	22.62	20.79	1.09	136.08	0.28	0.63 (12.6)	3.95 (79.0)	6.27	1.80	5.56
	-	49.46	53.23	0.93	292.05	0.59	0.76 (15.2)	3.80 (76.0)	5.00	3.25	9.23
SP2	+	28.44	18.63	1.53	164.83	0.33	0.61 (12.2)	3.68 (73.6)	6.03	2.33	7.30
	-	56.73	54.86	1.03	337.50	0.68	0.75 (15.0)	>4.00 (80)	>5.33	3.78	<16.93

\*Compressive strength of concrete ( $f_c$ ) = 30 MPa; Yielding strength of bar ( $f_y$ ) = 400 MPa

\*\*+ = Positive moment; - = Negative moment

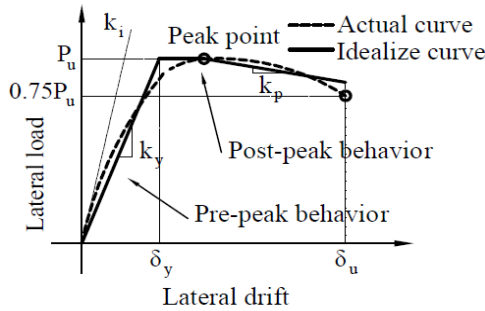


Fig. 17 Definition of the pre-peak and post-peak result (equal energy principle)

Figs. 16(a)-(b). The important extracted parameters from the results of the analysis, including load carrying capacity, deformation capacity and stiffness, are summarized in Table 5. The maximum resistances from the hysteresis diagrams in the two SP1 and SP2 were obtained at 1.5% drift. The maximum resistance from the numerical results is compared with the nominal resistance of the beam's flexural capacity in Table 5. To calculate the nominal resistance, the flexural capacity of the beam was multiplied in  $(L_b + h_c/2)$ , where  $L_b$  is the length of the beam and  $h_c$  is the depth of the column. The maximum joint shear value in Table 5 was obtained from the following equation.

$$V_{jmax} = P_{max} \times (L_b / j_d - (L_b + 0.5h_c) / L_c) \quad (9)$$

where  $L_c$  is the length of the column and  $j_b$  is the lever arm of coupling forces in the cross section of the beam. As can be seen in Table 5, in all the cases, the joint shear was less than its shear capacity ( $V_n$ ).

In order to obtain the parameters of deformation, their skeleton curve was used in real and idealized form on the basis of equal energy dissipation principle. This idealization is shown in Fig. 17. In the post-peak region after yielding, according to the ACI374.1-05 (2005) criteria, the equivalent deformation of 3/4 peak point was considered as the maximum displacement ( $\delta_u$ ) and the equivalent displacement of the yield resistance ( $\delta_y$ ) was obtained from the equal energy principle in pre-peak region by idealizing the actual curve with the bilinear curve. Moreover, for idealization of force-displacement curve in the post peak region, the straight line curve was used with its enclosed area equal to one in the actual curve. Ductility is defined as the ratio of  $\delta_u$  to  $\delta_y$  in the Table 5. In the SP2 under the negative moment, maximum drift was more than 4%, and

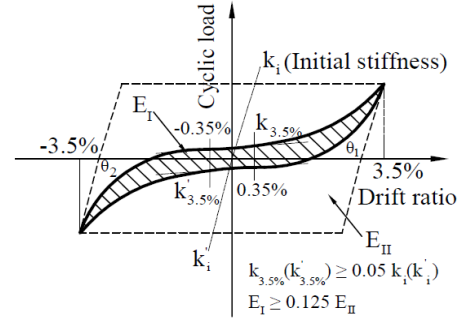


Fig. 18 Acceptance criteria for stiffness and energy dissipation specified by ACI374.1-05

therefore, the ductility obtained in this case was more than 5.33.

The parameters related to the connection stiffness are compared in Table 5. The initial line slope of the idealized curve considered as initial stiffness ( $k_y$ ) and slope of the straight line in the post peak region indicated as post peak stiffness ( $k_p$ ). The absolute value of post peak to initial stiffness ratio is shown in Table 5.

## 8.2 Assessment of connections performance in each cycle of loading

In order to evaluate the performance of connections in each cycle of loading, different parameters of the hysteresis curve connections were compared with ACI374.1-05 acceptance criteria. These parameters included degradation in load capacity, second stiffness ratio and energy dissipation ratio per cycle up to 3.5%. According to the ACI374.1-05 criteria, the moment resistance degradation in each cycle of loading after the maximum resistance should not be less than 25% for that direction of loading and the ratio of relative energy dissipation in each cycle should not be less than 1/8. As shown in Fig. 18, this ratio is obtained from the division of the enclosed area of the hysteresis diagram in each cycle of loading to the enclosed area of the dotted line. Moreover, the second stiffness in each cycle of loading should not be less than 0.05 of the initial stiffness in the first cycle. The second stiffness in each cycle is obtained from the slope of the passing line from -1/10 to +1/10 maximum drift of that cycle in Fig. 18.

To compare the parameters with the ACI374.1-05 criteria, the ratio of second stiffness to initial stiffness, resistance degradation to maximum resistance, energy

Table 6 Analysis results for comparison with the acceptance criteria in ACI374.1-05 for the SP1

Parameters	Load direction	Drift ratio (%)								
		0.25	0.5	0.75	1	1.5	2	3	4	3.5
Second stiffness ratio* (%)	Positive	100	91	66	52	31	11	5	4	4.5
	Negative	100	68	52	43	29	20	9	7	8.0
Load capacity degradation ratio*+ (%)	Positive	-	-	-	-	-	4	12	26	19.0
	Negative	-	-	-	-	-	7	19	26	22.5
Energy dissipation ratio*- (%)	-	28	15	10	13	18	20	20	19	19.5

\* Minimum allowable second stiffness ratio is 5% according to ACI 374.1-05.

\*+ Maximum allowable degradation in load capacity is 25% according to ACI 374.1-05.

\*- Minimum allowable energy dissipation ratio is 12.5% according to ACI 374.1-05.

Table 7 Analysis results for comparison with the acceptance criteria in ACI374.1-05 for the SP2

Parameters	Load direction	Drift ratio (%)								
		0.25	0.5	0.75	1	1.5	2	3	4	3.5
Second stiffness ratio* (%)	Positive	100	81	53	44	38	22	6	4	5.0
	Negative	100	97	69	57	46	19	14	7	10.5
Load capacity degradation ratio*+ (%)	Positive	-	-	-	-	-	7	17	29	23.0
	Negative	-	-	-	-	-	10	17	23	20.0
Energy dissipation ratio*- (%)	-	60	20	15	22	33	36	33	36	34.5

\* Minimum allowable second stiffness ratio is 5% according to ACI 374.1-05.

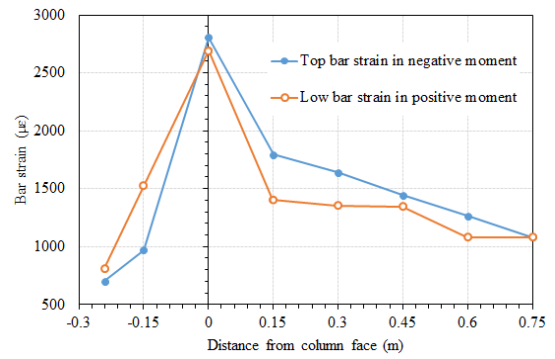
\*+ Maximum allowable degradation in load capacity is 25% according to ACI 374.1-05.

\*- Minimum allowable energy dissipation ratio is 12.5% according to ACI 374.1-05.

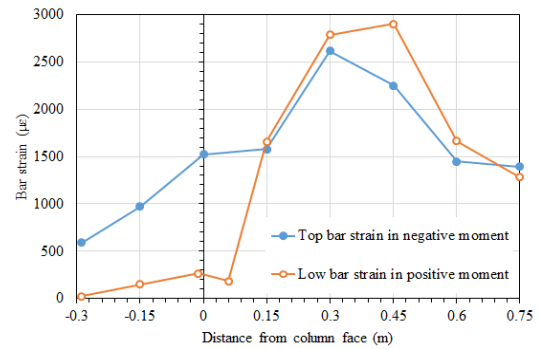
dissipation ratio in each cycle of loading for both the in-situ and precast connections are presented respectively in Tables (6)-(7). Values of 3.5% drift were obtained from the interpolation of the values of 3% and 4% drift. The results showed that in both type of the connections, except for the second stiffness ratio to initial stiffness under the positive moment at 3.5% drift ratio and energy dissipation at 0.75% drift ratio in the SP1, all the parameters were within the range.

### 8.3 Location of plastic hinge and crack distribution

To determine the location of plastic hinges, strain was measured at certain intervals from the column face. The strains were measured on longitudinal reinforcements or steel plates. In Figs. 19(a)-(b), the strains recorded from the SP1 and SP2 are shown. The measured strains were equivalent strains to maximum resistance under positive and negative moments. Strains of more than 2,000  $\mu\text{s}$



(a) SP1



(b) SP2

Fig. 19 The measured strain at the maximum resistance from the column face

indicated yielding of the reinforcement bars or steel segments in that region. In the SP1, all the strains were derived from the upper and lower reinforcing bars. As can be seen, in this joint, the concentration of plastic strains under the positive and negative moment was in the column face and by increasing distance from the column face, the strain of the reinforcement bar decreased and does not reach the yielding strain.

In the SP2 under a positive moment, the strain was recorded from the middle stiffener plate of the column steel tube. It was also measured at a distance of 60 mm from the column side in the bottom plate of the beam. The rest of the strains were measured in the upper and lower reinforcing bars of the beam. As shown in the Fig. 19(b), under the negative and positive moment, the maximum strain was respectively at a distance of 300 and 450 mm from the column face. Therefore, the location of the plastic hinge was located at a distance of 300 to 450 mm from there, which was out of the beam connection region. The length of the region in which the plastic strain occurred in the lower and upper reinforcements was more than that of the SP1, reflecting more utilization of the beam capacity in the SP2. As shown in the Fig. 19(b), plastic strain did not occur in the middle stiffener plate of the column steel tube and the bottom plate of the beam.

The forms of crack distribution in the SP1 and SP2 at 4% drift shown in Figs. 20(a)-(b), have the width larger than 0.1mm. As it is obvious, crack concentration in the SP1 has occurred in joint area. However in the SP2, crack distribution in the joint area has decreased and increased along the beam especially in the 20 to 70 cm from column

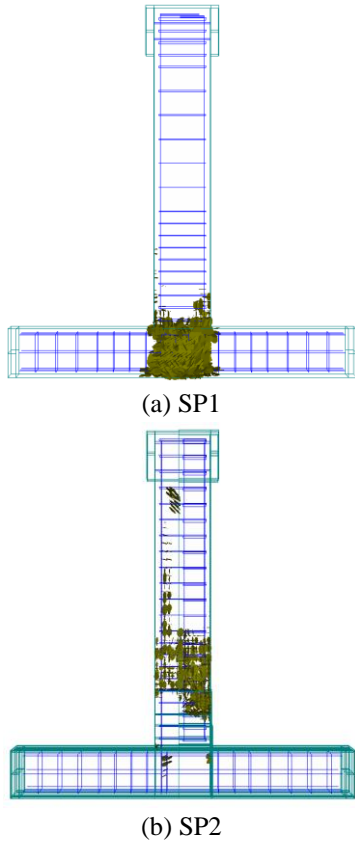


Fig. 20 Crack distribution and direction in 4% drift

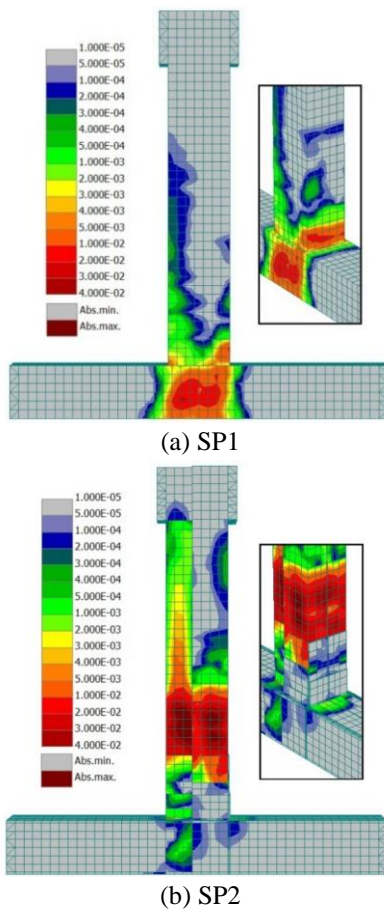


Fig. 21 Strain value at drift 4% in concrete and steel

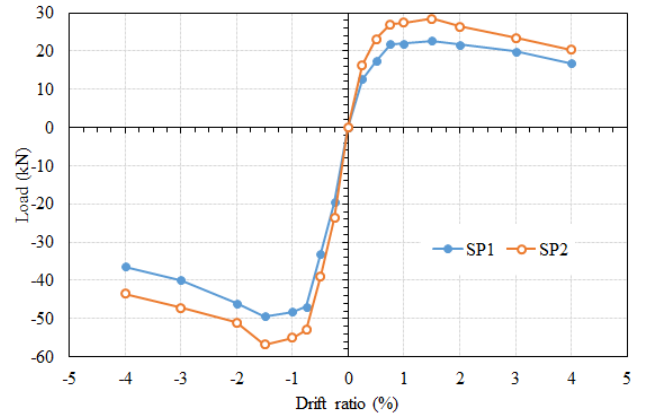


Fig. 22 Skeleton curves of the SP1 and SP2

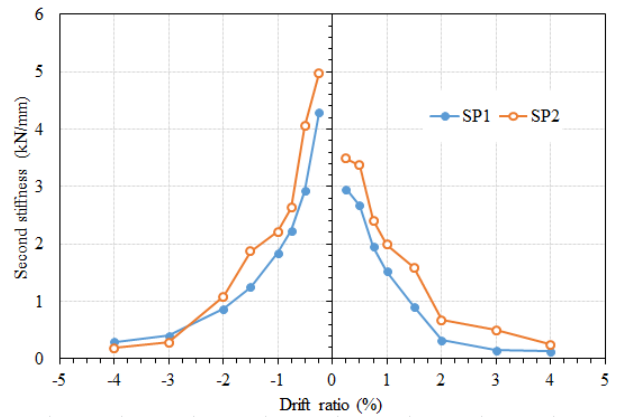


Fig. 23 Second stiffness of the hysteresis cycles of the SP1 and SP2

face.

The strain values at 4% drift in the steel and concrete parts are indicated in Figs. 21(a)-(b) for the SP1 and SP2. As it can be seen, the maximum strain of concrete is in accordance with the cracking pattern displayed in Fig. 20 but none of the steel parts including, bottom plates, side plates and steel tube reached to plastic strain ( $2000 \mu\text{s}$ ) in the SP2.

#### 8.4 Comparison of results

In order to compare the performance of the SP1 with SP2, the skeleton curves of these two connections are shown in Fig. 22. As can be seen the SP2 under the negative and positive moment has a higher resistance of about 26% and 15%, respectively. This higher resistance in the SP2 was due to the increase in the distance of plastic hinge location from the column face and decrease in the distance of lever arm from plastic hinge location to applied cyclic loading.

In order to compare the second and initial stiffness of the SP1 and SP2, the second stiffness in each cycle of the hysteresis diagrams is shown in Fig. 23. The stiffness of the 0.25% drift was the initial stiffness. The initial stiffness in the SP2 under the positive and negative moment was 1.18 and 1.16 times of the SP1, respectively. Moreover, except the 3 and 4% drift under the negative moment, the second

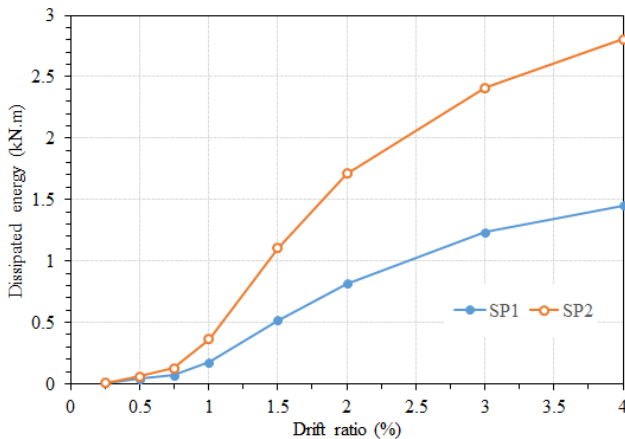


Fig. 24 Energy dissipation of the hysteresis cycles in both the SP1 and SP2

stiffness in all of the cycles in the SP2 is more than those of the SP1. It can be due to use of the steel tube in the joint area and bottom and sideway plates in the connection zone and the further confinement of concrete with them.

The energy dissipation of the connections, shown in Fig. 24, was obtained from the enclosed area of the hysteresis diagram in each cycle of the loading. As it is observed in all of the cycles except in the initial step, energy dissipation in SP2 was higher than the SP1. This higher energy dissipation was due to the utilization of a larger portion of the beam capacity. In addition, the concrete at the end of beam in the SP2 confined by the bottom and sideway plates as well as the concrete of the column joint confined by the steel tube experienced less damage during loading. Hence, the pinching in the hysteresis diagram particularly in the positive moment region in the SP2 was less and it had more energy dissipation than the SP1.

## 9. Conclusions

The most important challenge facing PRCS, by regarding the used precision in the construction of its elements, is how to connect these members in the workplace. The application of previous conventional PBC has less strength and ductility in comparison with IBC. In this study, it was attempted to keep the simplicity and efficiency in the manufacture, transportation and erection of prefabricated parts, while eliminating the undesirable performance of the PRCS with the innovated PBC. Summary results of the studied connections can be presented as follows:

1. The proposed PBC in addition to ease the production and erection processes, by having a comparable performance with IBC, can be used as an intermediate moment resistant connection in precast concrete structures.
2. The proposed PBC was able to meet the ACI374.1-05 criteria for moment resistant connection in the cases of strength, energy dissipation, and second stiffness.
3. The proposed PBC in comparison with existing PBCs due to the elimination of the column corbel and avoid

the loss of ceiling heights can provide better performance during the building serviceability. Moreover, manufacturing the segments can be done more easily in the factory due to substituting the steel tube with corbel and eliminating the protruding parts of the column and dapped part of the beam.

4. The location of the plastic hinge in the proposed PBC, unlike the equivalent IBC, formed beyond the connection region with a distance, 300 to 450 mm from the column face. Also, the length of the plastic hinge in the precast joint was obtained more than that of the in-situ one.

5. Results showed that the proposed PBC under positive and negative moments with a maximum resistance of 1.26 and 1.15 times the strength of the equivalent IBC, and more stiffness and energy dissipation, has a better performance.

## References

- ACI 318-14 (2014), Building Code Requirements for Structural Concrete and Commentary, American Concrete Institute Committee, Farmington Hills, MI, USA.
- ACI 374.1-05 (2005), Acceptance Criteria for Moment Frames Based on Structural Testing and Commentary, American Concrete Institute Committee, Farmington Hills, MI, USA.
- Bradley, B.A., Dahkal, R.P., Mander, J.B. and Li, L. (2008), "Experimental multi-level seismic performance assessment of 3D RC frame designed for damage avoidance", *Earthq. Eng. Struct. Dyn.*, **37**(1), 1-20.
- CEB-FIP Model Code (1990), Committee Euro-International du Beton, Bulletin Information, No. 195, Lausanne, Switzerland.
- Chen, W.F. and Saleeb, A.F. (1982), *Constitutive Equations for Engineering Materials*, Wiley, New York, USA.
- Cheng, C.T. (2008), "Seismic behaviour of post tensioned precast reinforced concrete beam-to-column connections", *Comput. Concrete*, **5**(6), 525-544.
- Choi, H., Choi, Y. and Choi, C. (2013), "Development and testing of precast concrete beam-to-Column connections", *Eng. Struct.*, **56**, 1820-1835.
- Fan, L. and Lu, X. (2008), "Investigation on seismic behaviour of jointed precast concrete frame structures", *The 14 World Conference on Earthquake Engineering*, Beijing, China, October.
- Ghayeb, H.H., Razak, H.A. and Sulong, N.H.R. (2017), "Development and testing of hybrid precast concrete beam to column connection under cyclic loading", *Constr. Build. Mater.*, **151**, 258-278.
- Guan, D., Guo, Z., Xiao, Q. and Zheng, Y. (2016), "Experimental study of a new beam-to-column connection for precast concrete frames under reversal cyclic loading", *Adv. Struct. Eng.*, **19**(3), 529-545.
- Hawileh, R.A., Rahman, A. and Tabatabai, H. (2010), "Nonlinear finite analysis and modelling of a precast hybrid beam-column connection subjected to cyclic loads", *Appl. Math. Model.*, **34**(9), 2562-2583.
- Hong, W., Kim, S., Park, S., Kim, J., Lee, S., Yoon, K. and Kim, S. (2010), "Composite beam composed of steel and precast concrete (modularized hybrid system)", *Struct. Des. Tall Spec. Build.*, **19**, 707-727.
- Hordijk, D.A. (1991), "Local approach to fatigue of concrete", Ph.D. Dissertation, Delft University of Technology, Delft, Netherlands.
- Im, H., Park, H. and Eom, T. (2013), "Cyclic loading test for

- reinforced-concrete-emulated beam-column connection of precast concrete moment frame”, *ACI Struct. J.*, **110**(1), 115-125.
- Kataoka, M.N., Ferreira, M.A. and EI Debs, A.L.H.C. (2015), “Study on the behaviour of beam-column connection in precast concrete structure”, *Comput. Concrete*, **16**(1), 163-178.
- Kupfer, H.B. and Gerstle, K.H. (1973), “Behaviour of concrete under biaxial stress”, *ASCE J. Eng. Mech. Div.*, **99**(4), 853-866.
- Lee, H.J. and Yu, S.Y. (2009), “Cyclic response of exterior beam-column joints with different anchorage methods”, *ACI Struct. J.*, **106**(3), 329-339.
- Maya, L., Zanuy, C., Albajar, L., Lopez, C. and Portabella, J. (2013), “Experimental assessment of connections for precast concrete frames using ultra high performance fiber reinforced concrete construction”, *Constr. Build. Mater.*, **48**, 173-186.
- PCI Hand Book (2010), Precast and Prestressed Concrete Institute, Design Handbook, PCI Industry Handbook Committee, Chicago, IL, USA.
- Rodriguez, M.E. and Torres, M.M. (2013), “Seismic behaviour of a type of welded precast concrete beam-to-column connection”, *PCI J.*, **73**(3), 81-94.
- Standard No. 2800 (2014), Iranian Code of Practice for Seismic Resistant Design of Buildings, Iranian Building Codes and Standards, Tehran, Iran.
- Van Mier, J.G.M. (1986), “Multi-axial strain-softening of concrete, part I: fracture, part II: load histories”, *Mater. Struct.*, **19**(111), 179-191.

AW